

Full-Sky Analysis of Cosmic-Ray Anisotropy with IceCube and HAWC

The HAWC Collaboration¹, The IceCube Collaboration²

¹ www.hawc-observatory.org/collaboration/icrc2015.php

² http://icecube.wisc.edu/collaboration/authors/icrc15_icecube

E-mail: juancarlos@icecube.wisc.edu

During the past two decades, experiments in both the Northern and Southern hemispheres have observed a small but measurable energy-dependent sidereal anisotropy in the arrival direction distribution of galactic cosmic rays. The relative amplitude of the anisotropy is $10^{-4} - 10^{-3}$. However, each of these individual measurements is restricted by limited sky coverage, and so the pseudo-power spectrum of the anisotropy obtained from any one measurement displays a systematic correlation between different multipole modes C_ℓ . To address this issue, we present the preliminary status of a joint analysis of the anisotropy on all angular scales using cosmic-ray data from the IceCube Neutrino Observatory located at the South Pole (90° S) and the High-Altitude Water Cherenkov (HAWC) Observatory located at Sierra Negra, Mexico (19° N). We describe the methods used to combine the IceCube and HAWC data, address the individual detector systematics and study the region of overlapping field of view between the two observatories.

Corresponding authors: Juan Carlos Díaz-Vélez^{1a,b*}, Dan Fiorino^{2a}, Paolo Desiati^a, Stefan Westerhoff^a, Eduardo de la Fuente^b

¹ juancarlos@icecube.wisc.edu

² dan.fiorino@icecube.wisc.edu

^aWisconsin IceCube Particle Astrophysics Center (WIPAC) and Department of Physics, University of Wisconsin–Madison, Madison, WI 53706, USA

^bCentro Universitario de Ciencias Exactas e Ingenierías, y Centro Universitario de los Valles, Universidad de Guadalajara, Guadalajara, Jalisco 44130, México

*The 34th International Cosmic Ray Conference,
30 July- 6 August, 2015
The Hague, The Netherlands*

*Speaker.

1. Introduction

Over the last few decades, several studies have measured appreciable variation in the intensity of cosmic rays of medium and high energies as a function of right ascension. An anisotropy with an amplitude of 10^{-4} was first observed at energies of order 1 TeV by a number of experiments including the Tibet AS γ [1], Super-Kamiokande [2], Milagro [3], EAS-TOP [4], MINOS [5], ARGO-YBJ [6], and HAWC [7] experiments in the Northern Hemisphere and IceCube [8, 9, 10] and its surface air shower array IceTop [11] in the Southern Hemisphere. In both hemispheres, the observed anisotropy has two main features: a large-scale structure with an amplitude of about 10^{-3} , and a small-scale structure with an amplitude of 10^{-4} with a few localized regions of cosmic-ray excesses and deficits of angular size 10° to 30° .

The origin of this anisotropy is not yet well understood since it is expected that cosmic rays should lose any correlation with their original direction due to diffusion as they traverse through interstellar magnetic fields. There are several theories regarding the possible origin of this anisotropy including ones that postulate a heliospheric origin [12, 13] though it is also possible that the origin of anisotropy is due to characteristics of the interstellar magnetic field at distances less than 1 parsec or even the diffuse flow of nearby galactic sources [14]. Others have proposed scenarios where the anisotropy results from the distribution of cosmic ray sources in the Galaxy and of their diffusive propagation [15, 16, 17, 18, 19, 20, 21].

IceCube and HAWC data can be combined at the same energy to study the full-sky anisotropy. Important information can be obtained on the power spectrum at low- ℓ (large scale), which is the region most affected by partial sky-coverage of one experiment only.

2. The Dataset

IceCube is a km³ neutrino detector located at the geographic South Pole. It is composed of 5160 Digital Optical Modules (DOMs) deployed at depths between 1450 m and 2450 m below the surface of the ice sheet. It detects the Cherenkov radiation emitted by relativistic charged particles as they propagate through the ice. The event rate varies between 2 kHz and 2.4 kHz, with the modulation caused by seasonal variations of the stratospheric temperature. The detected muon events are generated by primary cosmic-ray particles with median energy of 20 TeV, as determined by simulations. The estimated median angular resolution for this dataset from simulation is 3° [22].

The HAWC Observatory is a 22,000 m² dense array of 250 water Cherenkov detectors (WCDs) with 1200 photomultipliers (PMTs). Each WCD contains four photomultipliers per tank: one central high-quantum-efficiency 10-inch PMT and three 8-inch PMTs. The trigger rate in HAWC-250 is approximately 16 kHz. With 250 WCDs the angular resolution of the air shower reconstruction is between 0.3° and 1.5° . Poorly reconstructed events are reduced by requiring at least 6% of the PMTs are hit. From simulations we estimate that the median energy of the data set is about 2 TeV [23].

Data selected for preliminary analysis come from the third year of IceCube in its final configuration of 86 strings (IC86), as well as four months of HAWC in its preliminary configuration of 250 tanks (HAWC-250). Table 1 shows the characteristics of both detectors next to each other. Only continuous sidereal days of data were chosen for these analyses in order to reduce the bias

of uneven exposure along right ascension. For the purpose of studying systematics effects, we also use data from the HAWC-111 configuration that was collected between June 2013 and February 2014 by HAWC, when the observatory was operated with 111 WCDs during detector construction. The changing detector configuration within the HAWC-111 dataset makes it difficult to get a good energy estimation and is thus not suitable for the overall analysis. Figure 1 shows the distribution of data as a function of declination. There is a very narrow region of overlap between the two detectors. The statistics in HAWC-250 are comparable to one year of IC86. As evident from Table 1, there is also a difference in median energy of both experiments. A further complication is that the median energy grows as a function of zenith angle so that the region of overlap corresponds to the maximum median energy of both detectors. Figure 2 show this dependency and illustrates the way to select consistent data between the two detectors.

	IceCube	HAWC
Hemisphere	Southern	Northern
Latitude	-90°	19°
Trigger rate	2.5 kHz	10 kHz
Detection method	muons produced by CR and neutrinos	cascades produced by CR and γ
Median primary energy	10 TeV	2 TeV
Approx. angular resolution	2° – 3°	0.3° – 1.5°
Field of view	-90°/-20°, ~ 4 sr (always observes the same sky)	-30°/64°, ~ 2 sr (8 sr observed)
Livetime	362.2 days (6.2×10^{10} events)	52 days (3.3×10^{10} events)

Table 1: Comparison of the IceCube and HAWC datasets.

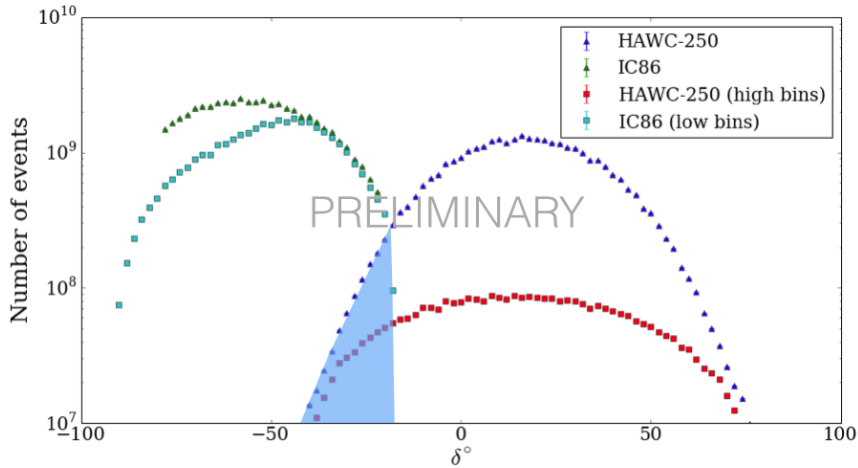


Figure 1: Distribution of events as a function of declination for IceCube and HAWC. The shaded area corresponds to the overlapping region for both experiments. Triangles correspond to the full energy spectrum and squares correspond to the same datasets after applying energy cuts. Restricting datasets to overlapping energy bins significantly reduces statistics for HAWC.

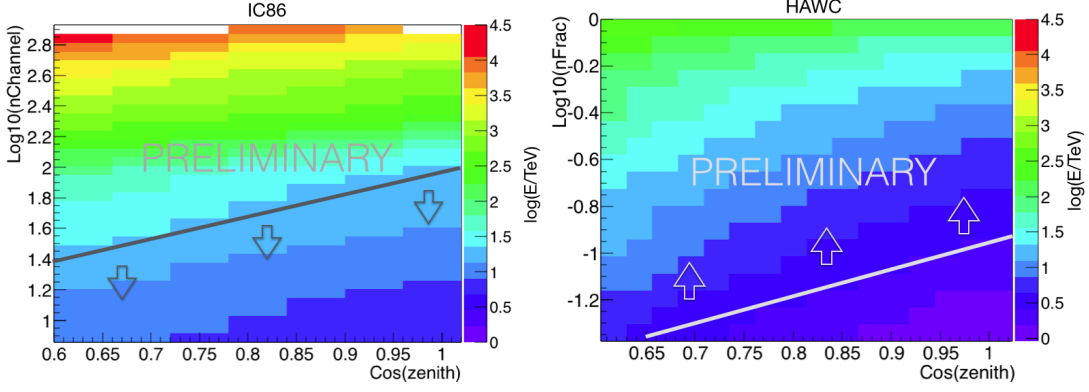


Figure 2: Energy cuts for IceCube (left) and HAWC (right) datasets. The two figures show the logarithm of the mean energy as a function of cosine zenith angle and number of hit channels (IceCube) or fraction of hits to number of available channels (HAWC) used as an energy proxy. Data are selected such that the two datasets are compatible with a median energy of 10 TeV.

3. Analysis

We compute the relative intensity as a function of equatorial coordinates (α, δ) by binning the sky into an equal-area grid with a resolution of 0.2° per bin using the HEALPix library [24]. In order to produce residual maps of the anisotropy of the arrival directions of the cosmic rays, we must have a description of the arrival direction distribution if the cosmic rays arrived isotropically at Earth $\langle N \rangle(\alpha, \delta)_i$. We calculate this expected flux from the data themselves in order to account for rate variations in both time and viewing angle. While the estimation of this reference map is calculated differently in IceCube and HAWC, these two methods are compatible. For HAWC, it is produced using the direct integration technique as described in [23], and in the case of IceCube the same is accomplished by time-scrambling events in local coordinates [8] within a time window Δt . Once the reference map is obtained, we calculate the deviations from isotropy by computing the relative intensity

$$\delta I(\alpha, \delta)_i = \frac{N(\alpha, \delta)_i - \langle N \rangle(\alpha, \delta)_i}{\langle N \rangle(\alpha, \delta)_i}, \quad (3.1)$$

where $N(\alpha, \delta)_i, \langle N \rangle(\alpha, \delta)_i$ are the number of observed events and the number of reference events in the i^{th} bin of the map, respectively. The relative intensity gives the amplitude of deviations from the isotropic expectation in each angular bin i .

This analysis method can be sensitive to any maximum angular scale through the choice of Δt . Due to the sampling of the reference map along lines of right ascension, the maximum angular scale shrinks as $1/\cos(\delta)$. Only a choice of 24 hours ensures a uniform angular scale as a function of δ . To eliminate larger structures, a multipole fit can be subtracted to access lower angular scales while preserving the maximum angular scale throughout the map.

Analyses of data from Earth-based experiments with partial sky coverage suffer from systematic effects and statistical uncertainties of the calculated angular power spectrum. An additional limitation is the fact that the combined map will suffer from the fact that this analysis is only sensitive to projections of large-scale structure onto the right ascension.

3.1 Systematic Checks

Sidereal anisotropy can be distorted by a yearly modulation in solar time unless the data are uniformly distributed over an integer number of complete years. One such modulation is the “solar dipole”, an observable anisotropy induced by the motion of the Earth through the Solar wind. The frame referred to as “anti-sidereal” time is a non-physical reference system which is obtained by inverting the sign on the conversion of solar time to sidereal time (adding 4 minutes per solar day) so the anti-sidereal year has 364.25 days. This anti-sidereal time frame can be used to study systematic effects caused by seasonal variations [25]. We produce a skymap where anti-sidereal time is used instead of sidereal time in the coordinate transformation from local detector coordinates to “equatorial” coordinates. Figure 3 shows the distribution of the relative intensity of CR under anti-

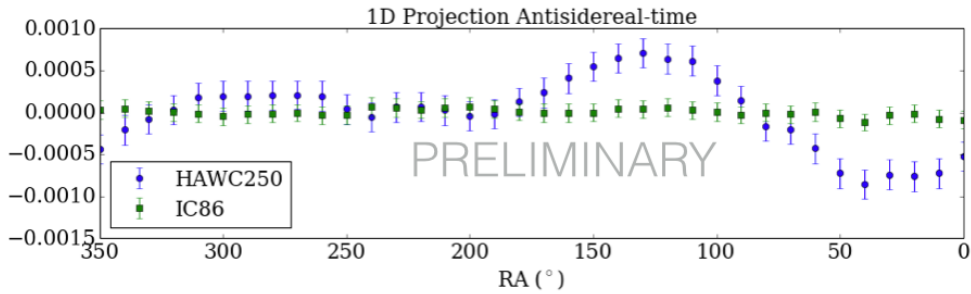


Figure 3: One-dimensional projection of the relative intensity of cosmic rays within the overlapping δ region (between -30° and -20°) as a function of RA as defined in the anti-sidereal coordinate system, a non-physical reference system that is obtained by inverting the sign on the conversion of solar time to sidereal time. This frame can be used to study systematic effects caused by seasonal variations. The presence of a seasonal effect such as a solar dipole is apparent in the HAWC-250 dataset as a significant deviation from a flat distribution.

sidereal reference. There is an apparent modulation in the HAWC data due to the fact that these data do not cover a full year. The effect of this modulation can be seen in the large-scale anisotropy when compared to IC86. Figure 4 shows the one-dimensional projection in right ascension for HAWC-111 and HAWC-250 compared to IC86. HAWC-111 (which covers a larger portion of a sidereal year) shows better agreement with IC86 while HAWC-250 shows a significant deviation in phase. Better agreement is expected with the accumulation of more statistics though, since the two experiments are observing different portions of the sky, there is no expectation that there should be perfect agreement. Figure 5 shows the power spectrum obtained from each dataset individually and was calculated with the method described in [10] and [7]. The missing C_ℓ for low ℓ is an artifact of the method that rises due to the limited sky coverage of the data.

4. Discussion and Future Plans

Current statistics for HAWC-250 are much lower than those of IC86 and do not comprise a full year. This limited coverage results in contamination from the solar dipole that can be observed in anti-sidereal coordinates. While HAWC-250 has a higher trigger rate than IceCube, restricting

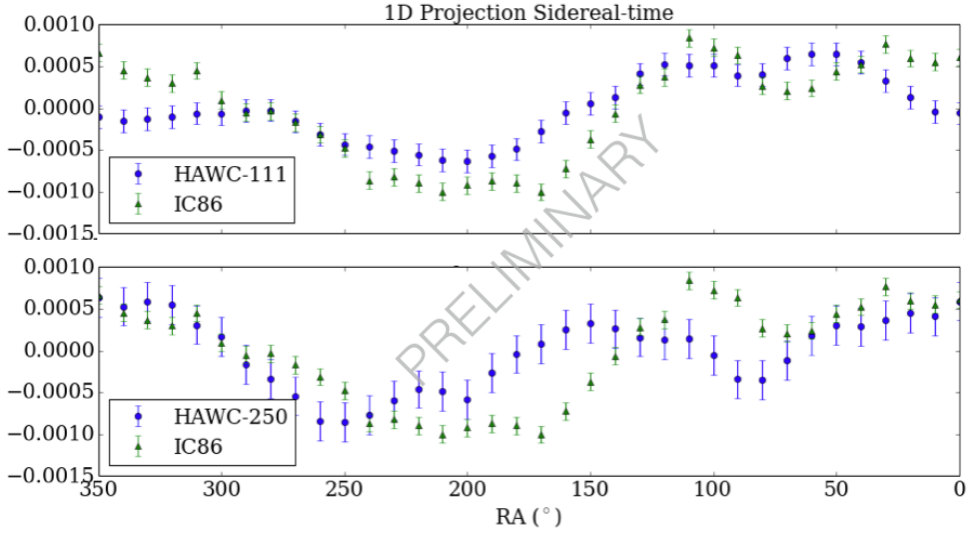


Figure 4: One-dimensional RA projection of the relative intensity of cosmic rays within the overlapping δ region (between -30° and -20°) for HAWC-111 (top) and HAWC-250 (bottom) compared to IC86 data. HAWC-111 (which covers a larger portion of a year) shows better agreement with IC86 while HAWC-250 shows a significant deviation in phase. Better agreement is expected with the accumulation of more statistics though some small-scale differences can be expected as a result of contamination from mis-reconstructed events belonging to other declination bands.

datasets to compatible energy bins reduces statistics for HAWC by nearly a factor of 10. This means that ~ 3 years of HAWC-250 are needed in order to have statistics equivalent to 1 year of IC86 in the energy range of interest.

Additional work is needed in order to understand differences in the two datasets in terms of mass composition and energy distribution. For example, the IceCube detector observes cosmic-ray air showers through TeV muons which travel on the order of 1 km through the South Pole ice sheet. At the energy threshold of this analysis, the IceCube detector will preferentially trigger on proton events over heavier nuclei (which produce lower energy muons on average) [10]. Recent measurements also indicate that the TeV band is a complex region of changing cosmic-ray composition, with protons becoming the sub-dominant primary type at energies above 10 TeV [26, 27]. As a result, IceCube and HAWC may not be observing a completely equivalent population of cosmic rays.

5. Conclusions

We have performed a preliminary analysis of the cosmic-ray anisotropy at TeV energies by combining datasets from the IceCube Neutrino Observatory, in the Southern Hemisphere, and the HAWC gamma-ray observatory, in the Northern Hemisphere. The objective of this ongoing study is to eliminate systematic effects and statistical uncertainties of the calculated angular power spectrum that result from partial sky coverage in each individual dataset.

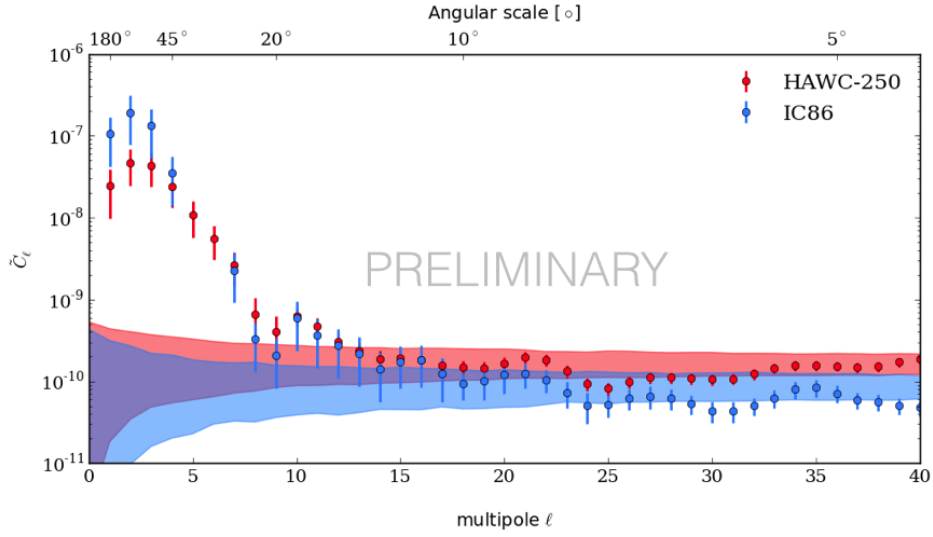


Figure 5: Power spectrum for IC86-III and HAWC-250 datasets. Solid color bands represent the power spectra for isotropic sky maps at the 90% confidence level.

Using limited statistics from the 250-tank configuration of HAWC and a full year of the 86-string configuration of IceCube, we observe both significant large-scale and small-scale anisotropy in the arrival direction distribution of TeV cosmic rays but note that the HAWC data are contaminated by the solar dipole that results from partial year coverage. It is expected that this main systematic bias should average out as we accumulate statistics and have a full year of HAWC data. Work is underway to identify and eliminate additional sources of systematic biases and incompatibilities between the data from the two detectors.

References

- [1] M. Amenomori et al., *Large-Scale Sidereal Anisotropy of Galactic Cosmic-Ray Intensity Observed by the Tibet Air Shower Array*, *Astrophys. J. Lett.* **626** (2005) L29–L32, [[astro-ph/0505114](#)].
- [2] G. Guillian et al., *Observation of the anisotropy of 10TeV primary cosmic ray nuclei flux with the Super-Kamiokande-I detector*, *Phys. Rev. D* **75** (2007) 062003, [[astro-ph/0508468](#)].
- [3] A. A. Abdo et al., *Discovery of Localized Regions of Excess 10-TeV Cosmic Rays*, *Phys. Rev. Lett.* **101** (2008) 221101, [[arXiv:0801.3827](#)].
- [4] M. Aglietta et al., *Evolution of the Cosmic-Ray Anisotropy Above 10^{14} eV*, *Astrophys. J. Lett.*, **692** (2009) L130–L133, [[arXiv:0901.2740](#)].
- [5] J. De Jong, *Observations of Large Scale Sidereal Anisotropy in 1 and 11 TeV cosmic rays from the MINOS experiment.*, *International Cosmic Ray Conference* **4** (2011) 46, [[arXiv:1201.2621](#)].
- [6] G. Di Sciascio, *Measurement of Cosmic Ray Spectrum and Anisotropy with ARGO-YBJ*, in *Euro. Phys. J. Web of Conf.*, vol. 52, p. 4004, 2013.
- [7] A. U. Abeysekara et al., *Observation of Small-scale Anisotropy in the Arrival Direction Distribution of TeV Cosmic Rays with HAWC*, *Astrophys. J.* **796** (2014) 108, [[arXiv:1408.4805](#)].

- [8] R. Abbasi et al., *Measurement of the Anisotropy of Cosmic-ray Arrival Directions with IceCube*, *Astrophys. J. Lett.* **718** (2010) L194–L198, [[arXiv:1005.2960](#)].
- [9] R. Abbasi et al., *Observation of Anisotropy in the Arrival Directions of Galactic Cosmic Rays at Multiple Angular Scales with IceCube*, *Astrophys. J.* **740** (2011) 16, [[arXiv:1105.2326](#)].
- [10] R. Abbasi et al., *Observation of Anisotropy in the Galactic Cosmic-Ray Arrival Directions at 400 TeV with IceCube*, *Astrophys. J.* **746** (2012) 33, [[arXiv:1109.1017](#)].
- [11] M. G. Aartsen et al., *Observation of Cosmic-Ray Anisotropy with the IceTop Air Shower Array*, *Astrophys. J.* **765** (2013) 55, [[arXiv:1210.5278](#)].
- [12] A. Lazarian and P. Desiati, *Magnetic reconnection as the cause of cosmic ray excess from the heliospheric tail*, *Astrophys. J.* **722** (2010) 188–196, [[arXiv:1008.1981](#)].
- [13] P. Desiati and A. Lazarian, *Anisotropy of TeV Cosmic Rays and Outer Heliospheric Boundaries*, *Astrophys. J.* (2013) 44.
- [14] P. Desiati and A. Lazarian, *Heliospheric Boundary and the TeV Cosmic Ray Anisotropy*, *J. Phys.: Conf. Ser.* (2014).
- [15] A. D. Erlykin and A. W. Wolfendale, *The anisotropy of galactic cosmic rays as a product of stochastic supernova explosions*, *Astroparticle Physics* **25** (2006) 183–194, [[astro-ph/0601290](#)].
- [16] P. Blasi and E. Amato, *Diffusive propagation of cosmic rays from supernova remnants in the Galaxy. II: anisotropy*, *JCAP* **1** (2012) 11, [[arXiv:1105.4529](#)].
- [17] V. Ptuskin, *Propagation of galactic cosmic rays*, *Astroparticle Physics* **39** (2012) 44–51.
- [18] M. Pohl and D. Eichler, *Understanding TeV-band Cosmic-Ray Anisotropy*, *Astrophys. J.* **766** (2013) 4, [[arXiv:1208.5338](#)].
- [19] L. G. Sveshnikova, O. N. Strelnikova, and V. S. Ptuskin, *Spectrum and anisotropy of cosmic rays at TeV-PeV-energies and contribution of nearby sources*, *Astropart. Phys.* **50** (2013) 33–46, [[arXiv:1301.2028](#)].
- [20] R. Kumar and D. Eichler, *Large-scale Anisotropy of TeV-band Cosmic Rays*, *Astrophys. J.* **785** (2014) 129.
- [21] P. Mertsch and S. Funk, *Solution to the Cosmic Ray Anisotropy Problem*, *Phys. Rev. Lett.* **114** (2015) 021101, [[arXiv:1408.3630](#)].
- [22] F. T. McNally, P. Desiati, and S. Westerhoff, *Study of Anisotropy in Cosmic-Ray Arrival Directions with IceCube and IceTop*, *ICRC 2015*.
- [23] S. Y. BenZvi, D. W. Fiorino, and S. Westerhoff, *Observation of Anisotropy in the Arrival Direction Distribution of TeV Cosmic Rays with HAWC*, *ICRC 2015*.
- [24] K. M. Górski et al., *HEALPix: A Framework for High-Resolution Discretization and Fast Analysis of Data Distributed on the Sphere*, *Astrophys. J.* **622** (2005) 759–771, [[astro-ph/0409513](#)].
- [25] F. J. M. Farley and J. R. Storey, *The sidereal correlation of extensive air showers*, *Proc. Phys. Soc.* **67** (1954) 996.
- [26] H. Ahn et al., *Discrepant hardening observed in cosmic-ray elemental spectra*, *Astrophys. J.* **714** (2010) L89.
- [27] Adriani et al., *PAMELA Measurements of Cosmic-Ray Proton and Helium Spectra*, *Science* **332** (2011) 69–72.